Plasma spraying of zirconia-reinforced hydroxyapatite composite coatings on titanium

Part I *Phase, microstructure and bonding strength*

E. CHANG, W.J. CHANG, B.C. WANG, C.Y. YANG*
Department of Materials Science and Engineering and Orthopaedics, National Cheng Kung University, Tainan, Taiwan 701*

Plasma-sprayed hydroxyapatite (HA) coatings applied to metal substrates can induce a direct chemical bond with bone and hence achieve biological fixation of the implant. However, the poor bonding strength between HA and substrate has been of concern to orthopaedists. In this study, two submicrometre ZrO_2 powders stabilized with both 3 and 8 mol % Y_2O_3 (TZ3Y and TZ8Y, respectively) were incorporated in a plasma-sprayed HA coating on Ti-6Al-4V substrate to investigate the change in phase, microstructure and bonding strength. The results show that ZrO_2 composite coatings contain more unmelted particles and greater porosity. During plasma spraying, ZrO_2 reacts with the CaO in HA to form $CaZrO_3$ and accelerates HA decomposition to α-TCP and $Ca_4P_2O_9$. Nevertheless, bonding strength increases with increase of ZrO_2 content in the range 0 to 10 wt % studied. The higher Y_2O_3-containing TZ8Y apparently exerts a greater strengthening effect than the lower Y_2O_3-containing TZ3Y.

1. Introduction

Previous experimental studies in animals and experiences with human implants have suggested that plasma-sprayed hydroxyapatite coatings (HAC) on metal substrates can induce a direct chemical bond with bone and hence achieve biological fixation of the implant [1–4]. Limited by the strength of hydroxyapatite *per se* [5], porosities and inclusions in the lamellar structure of the coating, and the residual stress in the coating, the bonding strength of the HAC/metal interface has been the point of potential weakness in prosthesis. Previous studies on the bonding between HAC and bone have shown the importance of the strength of hydroxyapatite (HA) in the coating [1,6,7].

It has been shown that a stress-induced phase transformation can be used to increase the strength of brittle materials, in which ZrO_2 is often added as a second phase [8–10]. Recently, ZrO_2 was used to toughen bulk HA and bioglass and the results showed promise for composite materials [11–13]. The present study aimed at employing the plasma spraying method to synthesize HA coatings reinforced by ZrO_2 of varying content. The microstructure and morphology of the coatings, the phase transformation during plasma spraying and the bonding strength were also investigated.

2. Materials and methods

2.1. Powder and specimen preparations

Powders of HA and two kinds of ZrO_2 (TZ3Y and TZ8Y) manufactured by Merck and Toyo Soda, respectively, were used. The chemical compositions of TZ3Y and TZ8Y are shown in Table I. Typical sizes of TZ3Y and HA (at 50% cumulative mass per cent) were measured as 0.2 μm and 7.0 μm (Sedigraph 5100), respectively, as shown in Fig. 1. The particle size distribution of TZ8Y is similar to TZ3Y. Mixtures of the following compositions were investigated: HA, HA + 5 wt % TZ3Y (3–5), HA + 10 wt % TZ3Y (3–10), and HA + 10 wt % TZ8Y (8–10). The HA and ZrO_2 were mixed in an attrition mill (Union Process) with ethanol as dispersant, and vacuum dried. The mixed powders were further granulated with 10 wt % of aqueous PVA solution (conc. at 5 wt %), sieved to −120− + 200 mesh (74–125 μm) and sintered at 600 °C for 1 h and 1000 °C for 4 h.

Two shapes of Ti-6Al-4V substrate (ASTM F-136) were used, one in plate form for microstructure and phase analyses and the other in cylindrical form for bonding strength measurements (ASTM C-633). All specimens were cleaned in acetone ultrasonically and then sand blasted to roughen the surface before plasma spraying with the prepared powders; the spraying parameters are shown in Table II.

2.2. Material characterization

The mixed powders before granulation were subjected to differential thermal analysis (DTA) (Setayam, Tag 24) at a heating rate of 5 °C/min to 1450 °C to investigate any possible reactions between HA and ZrO_2 that might occur during the subsequent sintering.

0957–4530

TABLE I Chemical compositions of the two ZrO_2 powders used

Composites	Composition (wt %)					
	ZrO_2	Y_2O_3	Al_2O_3	SiO_2	Fe_2O_3	Na_2O
TZ3Y	Balance	4.95	< 0.005	< 0.002	< 0.002	0.021
TZ8Y	Balance	13.26	< 0.005	< 0.006	< 0.002	0.057

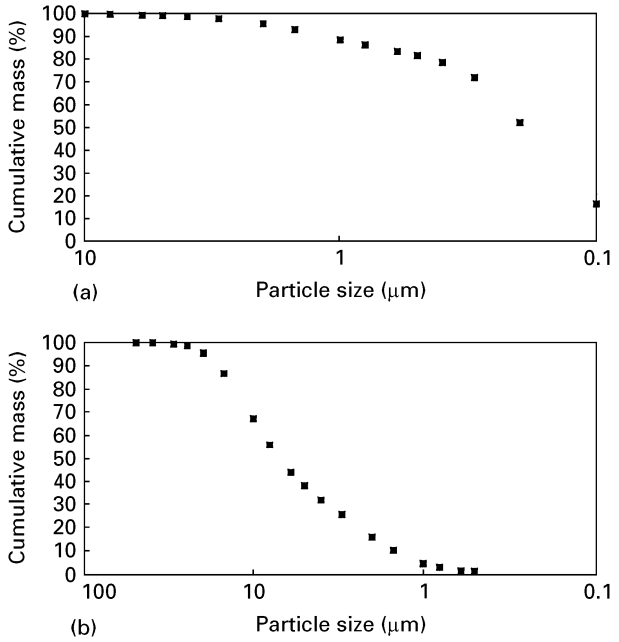

Figure 1 Cumulative mass per cent versus particle size of (a) TZ3Y and (b) HA powders.

TABLE II Plasma-spraying parameters for HA and ZrO_2/HA composites

Primary gas/flow rate (l/min)	Ar/41
Secondary gas/flow rate (l/min)	H_2/8
Powder carrier gas/flow rate (l/min)	Ar/3.2
Powder feed rate (g/min)	20
Power (kW)	40.2
Stand-off distance (cm)	7.5
Surface speed (cm/min)	2400
Transverse speed (cm/min)	60

Scanning electron microscopy (SEM) with wavelength-dispersive spectrometer (WDS) was used to observe the morphology of powder, coating surface, cross-sectional microstructure and element distribution. The phase identity was examined by X-ray diffractometer (XRD) (Rigaku D/Max III, V) using CuK_α radiation.

One inch diameter rod was used for the measurement of the bonding strength of the coatings per ASTM C-633. For specimen preparation, one rod was first sand-blasted and plasma-sprayed with a HA coating of 150 μm thickness. The coupling rod was also sand-blasted, glued with thermoplastic and then joined under pressure in a fixture to the rod with HA coating. The couples, cured at 190 °C for 2 h, were subjected to tensile tests at an extension rate of 0.02 mm/s until failure. The fracture structure was examined by optical microscope (OM) and SEM. For each testing material, five specimens were used, and the bonding strength data is reported as the average values.

3. Results and discussion

The results for low 2θ angle XRD analysis of TZ3Y and TZ8Y powders are shown in Fig. 2. This figure shows that the TZ3Y powder contains a minor monoclinic phase in addition to a cubic phase, while the TZ8Y powder is a pure cubic phase; XRD analysis at high 2θ angle (72–75°) confirms the existence of cubic phase. As the material is stressed ahead of a propagating crack, the submicrometre ZrO_2 will be destabilized to cause a transformation from cubic phase to monoclinic phase, which induces an approximately 9% volumetric increase of ZrO_2 and generates a compressive stress state to retard further crack growth [14]. Thus, the TZ8Y material with full cubic phase might exert a greater strengthening effect than the monoclinic-containing TZ3Y material. Fig. 3 shows

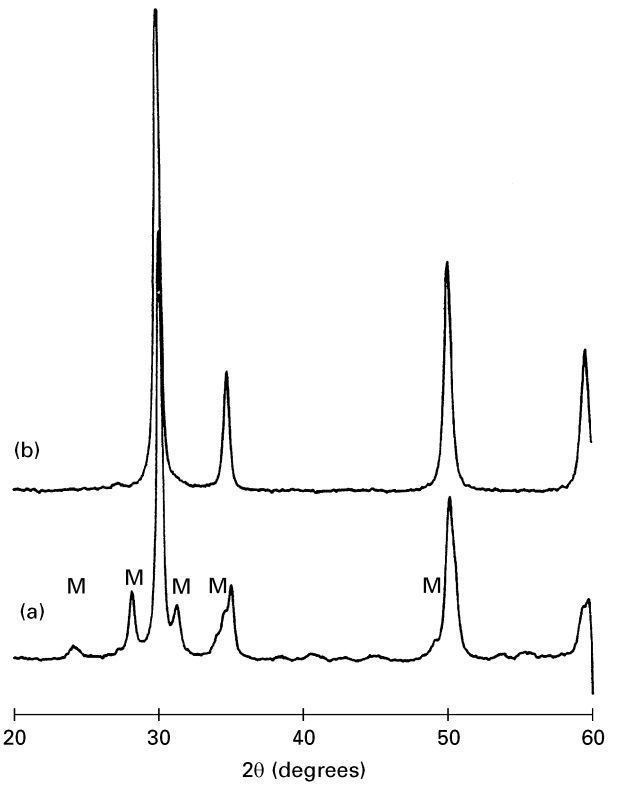

Figure 2 XRD results for (a) TZ3Y and (b) TZ8Y powders: *M* = monoclinic.

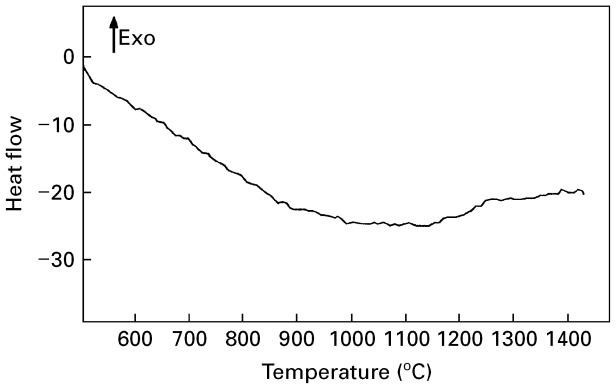

Figure 3 DTA result of the mixture of HA and TZ8Y powders.

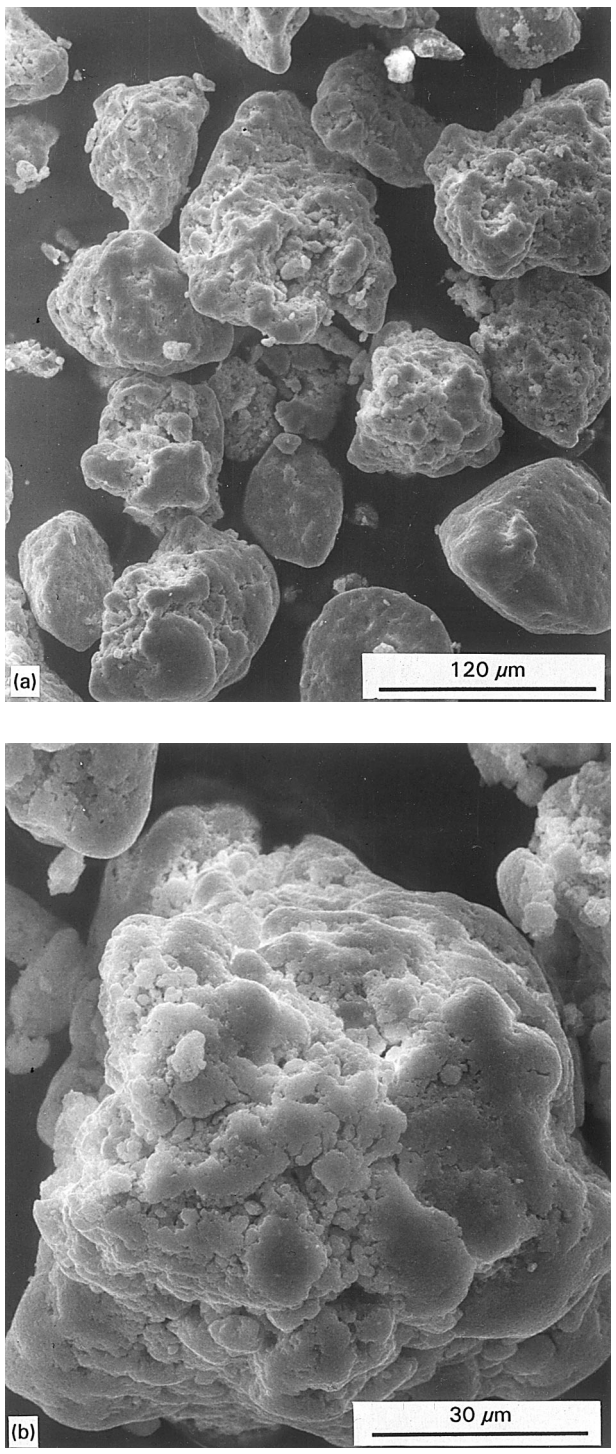

Figure 4 SEM morphology of the typical sintered granulated composite powders controlled at 74–125 μm: (a) ×250; (b) ×1000.

that the mixture of HA and TZ8Y powders exhibits no apparent endothermic or exothermic peaks upon heating to 1000 °C, and this result is supported by later XRD analyses of the sintered powders, which exhibit no phase decomposition in HA resulting from the reaction between HA and ZrO_2 during sintering. The morphology of sintered granulated powders consists of aggregates of particles as shown in Fig. 4. Sintering of particles is evident, and the spherical shape of the sintered powder controlled at 74–125 μm facilitates powder feeding.

The surface morphologies observed by SEM of plasma-sprayed HA and 8–10, 3–5 and 3–10 coatings are shown in Fig. 5. Comparison of the surface morphologies shows that the ZrO_2 composite coatings contain more unmelted small particles; apparently, the amount of unmelted particle increases with increase of ZrO_2 (comparing Fig. 5c and 5d). The SEM cross-sectional view, Fig. 6, shows that additions of ZrO_2 cause an increase in porosity of the materials. The rationale of higher porosity ZrO_2-added materials is thought to be due either to the higher melting point of ZrO_2 ($\sim$2680 °C) or the lower thermal conductivity of ZrO_2 ($\sim$1 w/m k) [15], while the melting point of HA is 1670 °C. As the content of ZrO_2 increases the heat of the plasma jet might be insufficient to melt the ZrO_2-reinforced HA powders. An even distribution of ZrO_2 in the HA coating might influence the strengthening effect. Fig. 7 shows the cross-sectional microstructure and WDS mapping of Zr elements, and based on the result it can be deduced that the ZrO_2 particles apparently distribute uniformly in HA without clustering.

Fig. 8 shows the XRD results for HA, 8–10, 3–5 and 3–10 materials before and after plasma spraying. After plasma spraying, α-, β-$Ca_3(PO_4)_2$ (or α-, β-TCP), $Ca_4P_2O_9$ and CaO impurity phases were identified, similar to a previous study [16]. In addition, the cubic ZrO_2 phase apparently was not altered during the fabrication process. The amount of impurity phases in the following is defined as the relative intensity of a specific phase to the main HA peak of the same specimen. The content of impurity phases using this definition is shown in Table III. This table shows that the addition of ZrO_2 results in an increase of α-TCP phase and a decrease of CaO phase.

Investigating hot pressed and hot isostatic pressed bulk ZrO_2/HA composite at 1050 °C, Ioku *et al.* [12] found that the CaO in HA diffuses into ZrO_2 to cause the tetragonal ZrO_2 to transform into cubic ZrO_2. The loss of CaO will then accelerate the decomposition of HA into β-TCP phase above 800 °C. The reaction of their study is expressed as follows:

$$\text{Y-}ZrO_2(T) + Ca_{10}(PO_4)_6(OH)_2 \rightarrow$$

$$\text{CaO doped Y-}ZrO_2(C)$$

$$+ 3\beta\text{-}Ca_3(PO_4)_2 + H_2O \quad (1)$$

Similar to the result of Ioku *et al.*, Tamari *et al.* [17] hot pressed bulk materials at 1300–1400 °C and also found the transformation of tetragonal ZrO_2 into cubic ZrO_2 phase after sintering; however, α-TCP was

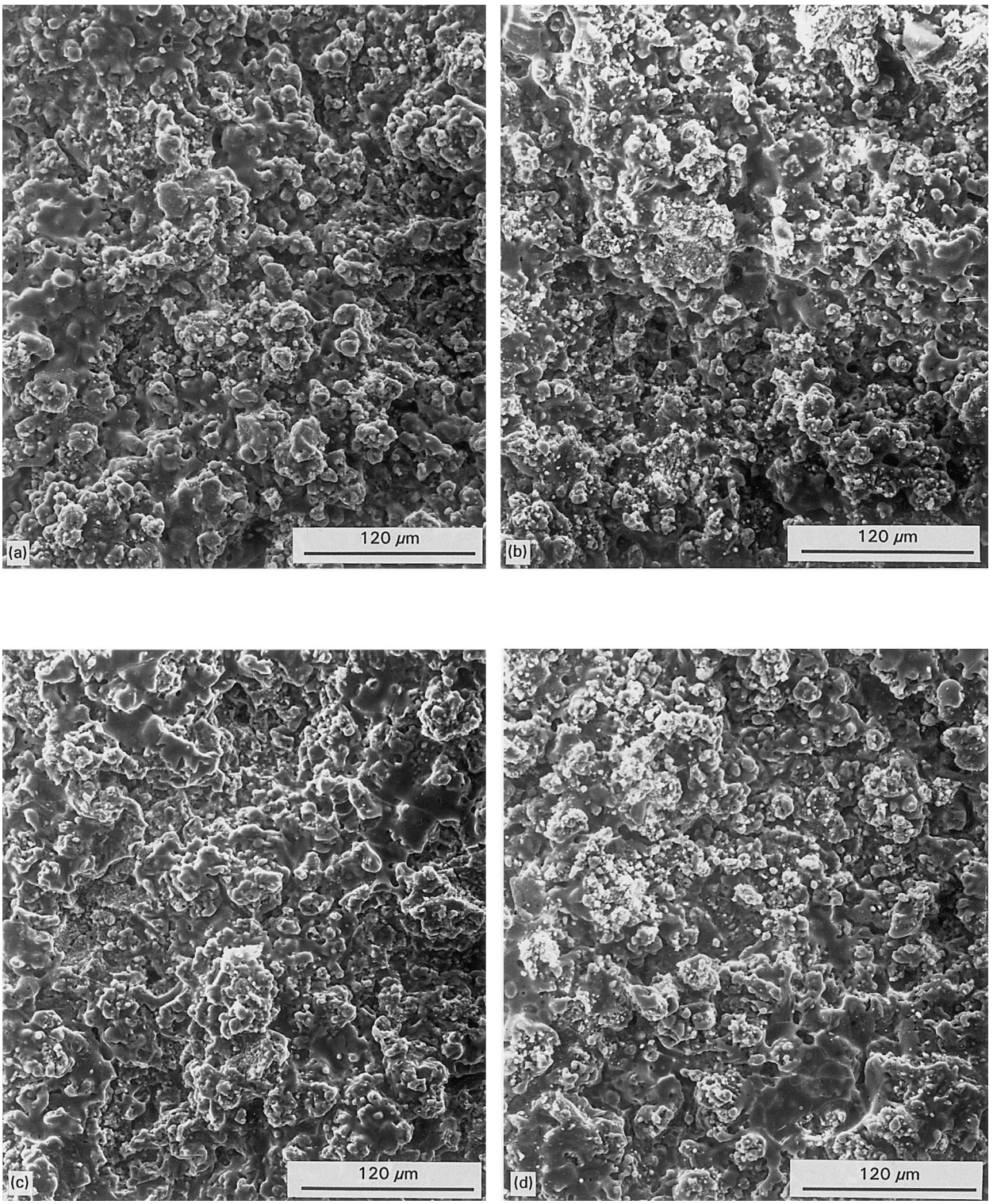

Figure 5 Surface morphologies observed by SEM of plasma-sprayed (a) HA, (b) 8–10, (c) 3–5 and (d) 3–10 coatings.

the decomposition product rather than β-TCP phase. They inferred that the following reactions occurred simultaneously:

$$Ca_{10}(PO_4)_6(OH)_2 \rightarrow 3\alpha\text{-}Ca_3(PO_4)_2 + CaO + H_2O \quad (2)$$

$$ZrO_2(T) + CaO \rightarrow CaO \text{ doped } ZrO_2(C) \quad (3)$$

Another study by Wu and Yeh [18] indicated that at sintering temperatures over 1150 °C, HA will decompose into β-TCP and CaO and ZrO_2 will further react with CaO to produce a new $CaZrO_3$ phase.

With a difference from the previous works on bulk materials [12, 17, 18], the present study by plasma spraying finds that the α-TCP phase in the coating increases, with an associated reduction of the CaO phase, and XRD analysis of the composite specimens failed to identify any reaction phases between HA and ZrO_2. To further elucidate the problem, the composite coatings were immersed in hydrochloric acid to

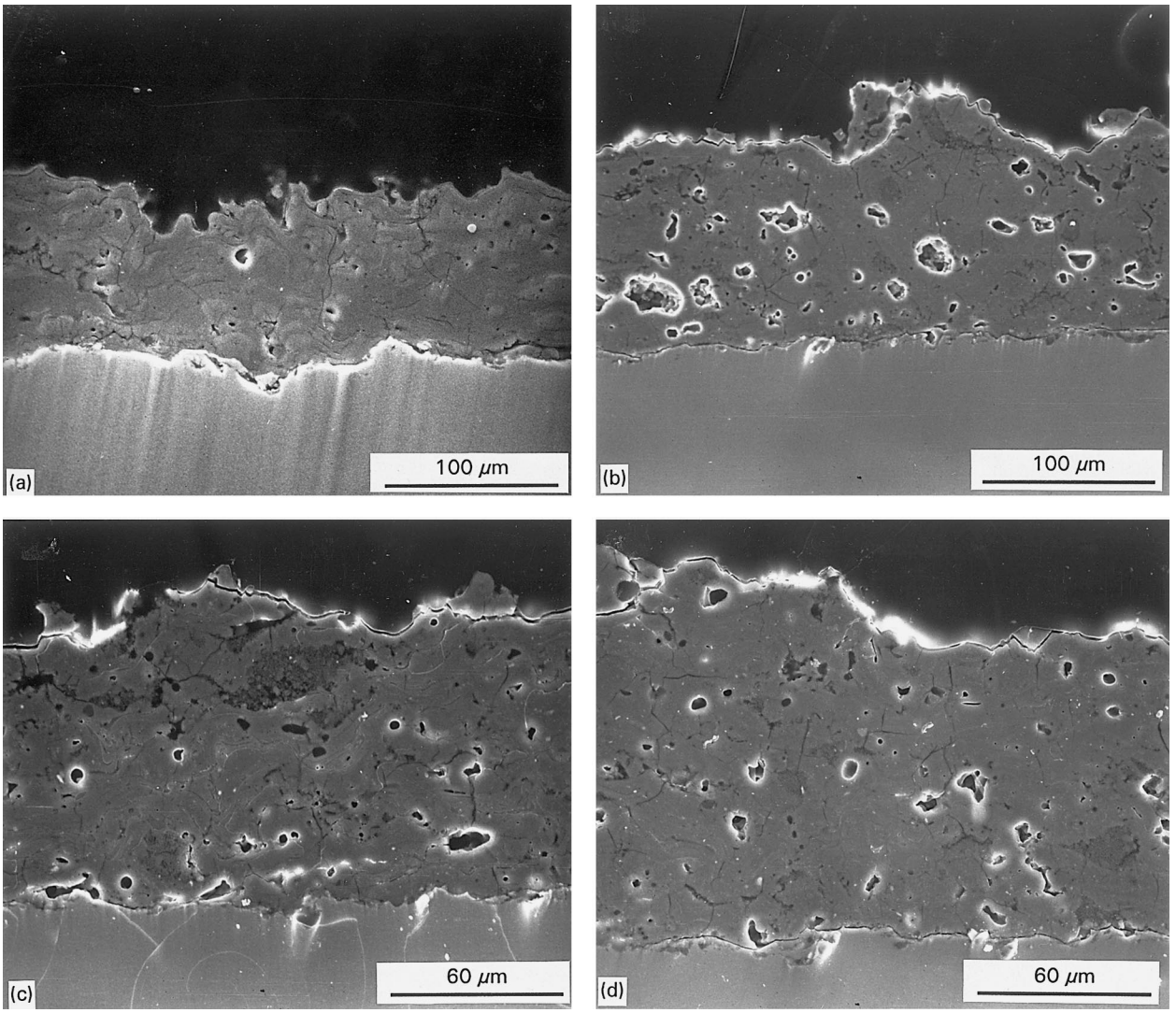

Figure 6 SEM cross-sectional microstructures of plasma-sprayed (a) HA, (b) 8–10, (c) 3–5 and (d) 3–10 coatings.

dissolve the soluble calcium phosphates, and then the residues were collected and analysed by XRD. Comparing Fig. 9a from the residues of the 8–10 specimen with the TZ8Y powders (Fig. 9b) clearly indicates the following: (1) the ZrO_2–8 wt % Y_2O_3 particles remained as cubic phase after plasma-spraying; and (2) a very small amount of $CaZrO_3$ phase was found.

The decomposition of HA and generation of impurity phases such as α-$Ca_3(PO_4)_2$, β-$Ca_3(PO_4)_2$, $Ca_4P_2O_9$ and CaO during plasma spraying has been reviewed [19]. With the addition of Y-ZrO_2, it is assumed that two additional reactions had taken place during plasma spraying: (1) ZrO_2 reacts with CaO in HA to form $CaZrO_3$; and (2) reduction of CaO in HA accelerates the decomposition of CaO-poor HA into α-TCP and minor $Ca_4P_2O_9$, and the high-temperature α-TCP phase remained at room temperature due to the fast cooling rate after plasma spraying. The additional HA reactions can be expressed as:

$$Ca_{10}(PO_4)_6(OH)_2 + ZrO_2 \rightarrow$$

$$\text{CaO-poor } Ca_{10}(PO_4)_6(OH)_2 + CaZrO_3 + H_2O \quad (4)$$

$$\text{CaO-poor } Ca_{10}(PO_4)_6(OH)_2 \rightarrow$$

$$2(1 + x)\alpha\text{-}Ca_3(PO_4)_2 + (1 - x)\,Ca_4P_2O_9 + H_2O \ (x = 0\text{–}1) \quad (5)$$

Equation 5 is responsible for the increase in α-$Ca_3(PO_4)_2$ found in this study. Direct reaction between HA and ZrO_2 to create the following reaction:

$$Ca_{10}(PO_4)_6(OH)_2 + ZrO_2 \rightarrow \alpha\text{-}Ca_3(PO_4)_2 + CaZrO_3 + H_2O \quad (6)$$

which increases the content of α-$Ca_3(PO_4)_2$ and generates $CaZrO_3$, is thought to be less likely. Equation 6 infers that α-$Ca_3(PO_4)_2$ and $CaZrO_3$ would have been produced in equal quantity (in moles), yet the reaction product of $CaZrO_3$ is scarce (Fig. 9). Although the temperature of the plasma jet was high, the time for the molten HA to react with ZrO_2 was limited, and hence the quantity of reaction product was small. This reaction might help to bond ZrO_2 to HA.

The results of bonding strength per ASTM C-633 is shown in Table IV: each value in the table represents an average of five test data. The following conclusions can be drawn from the measurements: (1) the pure HA coating shows the lowest bonding strength; (2) TZ8Y

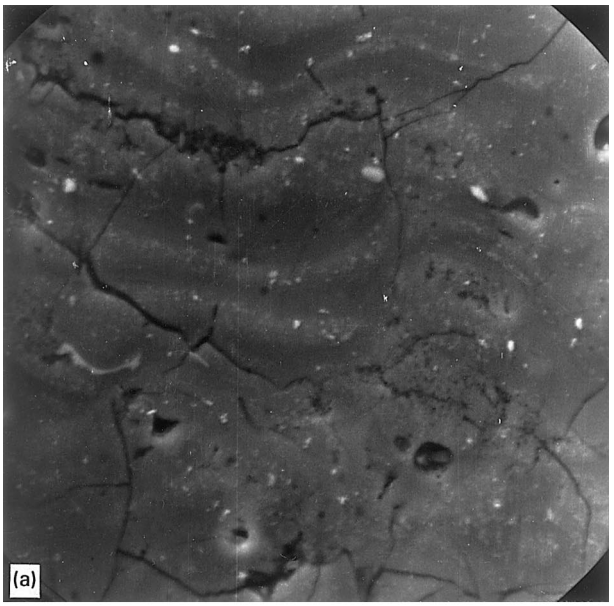

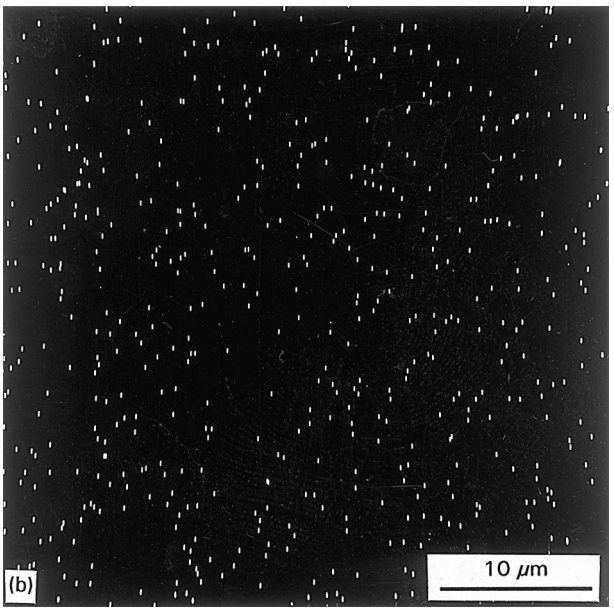

Figure 7 (a) SEM cross-sectional microstructure and (b) WDS mapping of the corresponding Zr element distribution in 8–10 specimen.

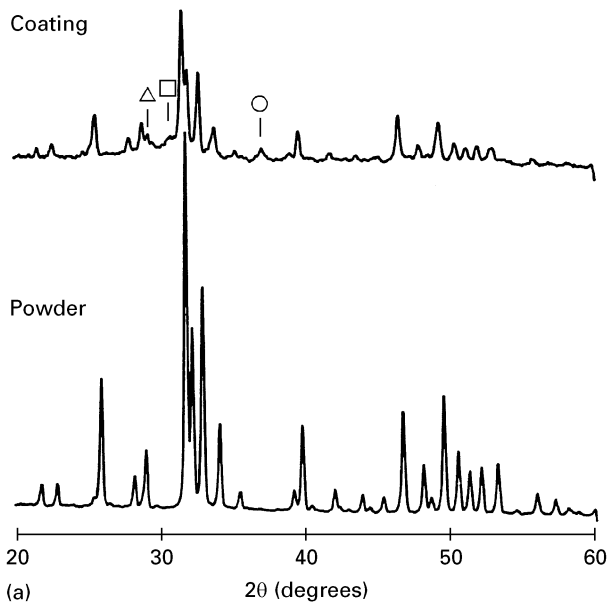

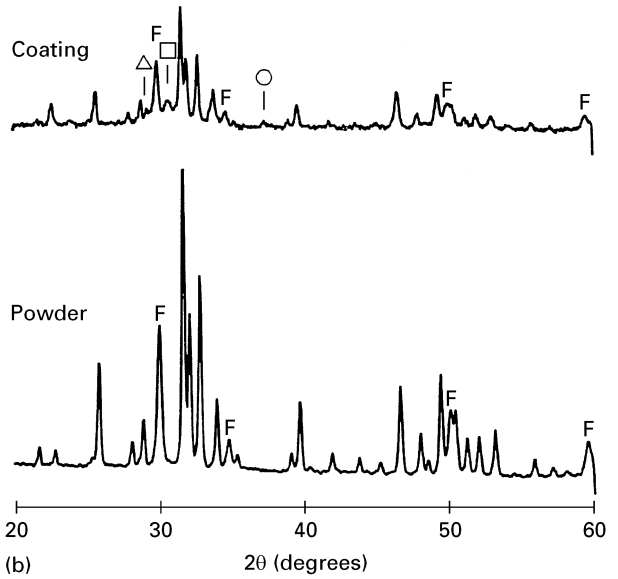

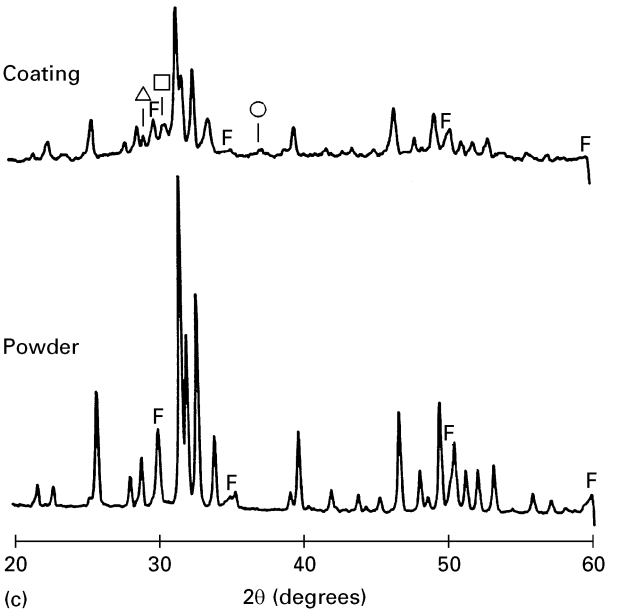

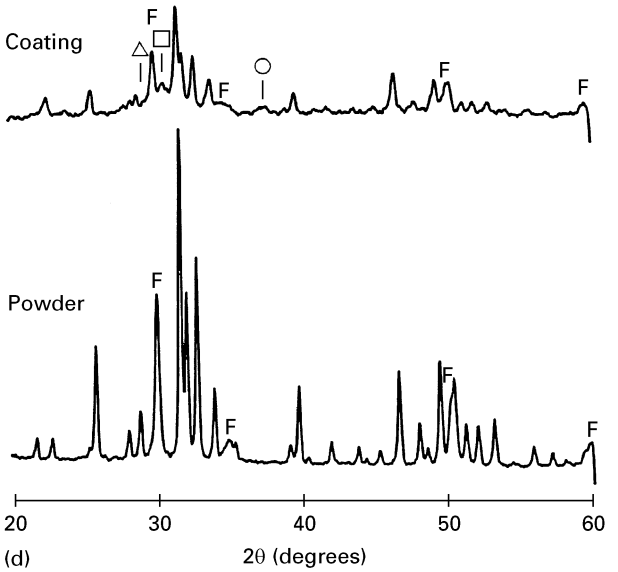

Figure 8 XRD results of (a) HA, (b) 8–10, (c) 3–5 and (d) 3–10 materials before and after plasma spraying: △ $Ca_4P_2O_9$; □ TCP; ○ CaO; F ZrO_2.

TABLE III Relative phase contents in HA and ZrO_2/HA coatings

Phase coating	α-TCP (%)	β-TCP (%)	$Ca_4P_2O_9$ (%)	CaO (%)
HA	15.09	7.87	7.05	12.85
8–10	40.39	8.16	9.52	7.08
3–5	30.37	7.53	9.02	6.47
3–10	38.90	7.48	8.56	6.27

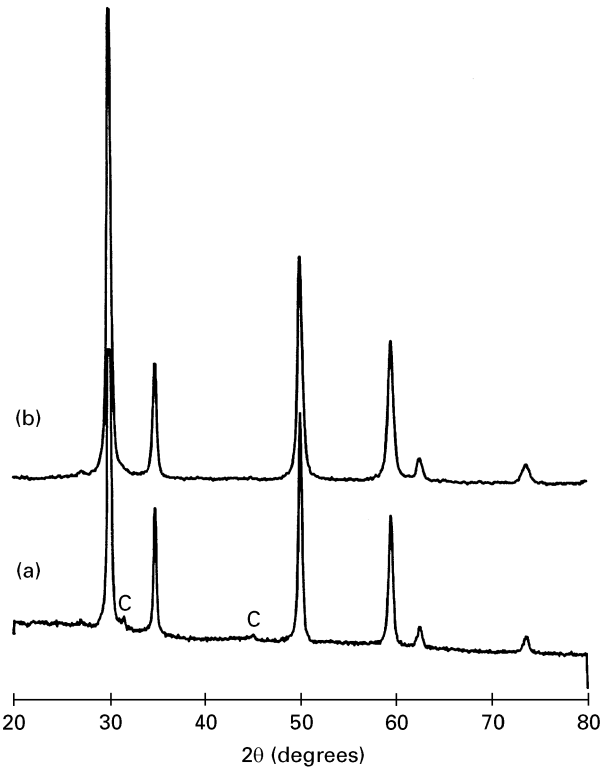

Figure 9 Comparison of XRD results between (a) residues from 8–10 specimen immersed in hydrochloric acid and (b) TZ8Y powders: C = $CaZrO_3$.

TABLE IV The bonding strength of HA and ZrO_2/HA composite coatings

Coatings	Bonding strength
HA	28.24 ± 3.68
8–10	32.49 ± 4.24
3–5	29.85 ± 2.46
3–10	31.95 ± 3.31

exerts a slightly higher strengthening effect than does TZ3Y; and (3) the bonding strength increases with increase of TZ3Y in the range 0 to 10 wt %. In addition to the toughening of HA induced by the transformation of ZrO_2 as mentioned previously [14], other mechanisms of crack deflection or branching might also contribute to the toughening of ceramics [20, 21].

Other factors of microstructures, such as porosity and microcracks, will certainly influence adversely the bonding strength of HA. In this study, the addition of ZrO_2 increases the porosity of the coatings (compare

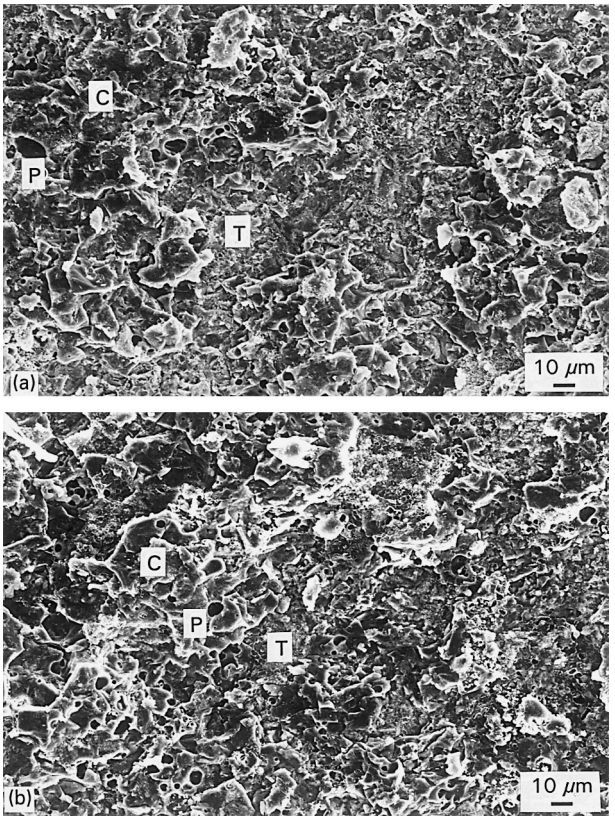

Figure 10 SEM fracture surface morphologies of (a) HA and (b) 8–10 specimens. T: Ti-6Al-4V, C: coating, P: porosity.

8–10, 3–5 and 3–10 coatings with the HA coating, Fig. 6). The result that the bonding strength increases with an increase of ZrO_2 indicates that, within 10 wt % addition, the positive effect of toughening by ZrO_2 outweighs the negative effect of increased porosity. The fracture surface of the four coatings investigated at optical microscope (OM) level shows a similar mixed mode failure occurring at the substrate–coating interface, the coating itself and the coating–glue interface. Observation of the fracture surface at SEM level, as shown in Fig. 10, shows a typical flake-like brittle fracture. On the surface, substrate and coating can be found confirming the mixed mode failure observed by OM. At present, differences in the characteristics of the four coatings cannot be elucidated.

4. Conclusions

With the aim of increasing the bonding strength between the HA and Ti-6Al-4V substrate for use in orthopaedic prosthesis, zirconia-reinforced hydroxyapatite materials were fabricated by a plasma-spraying method. In addition, such properties of coatings as phase, microstructure and bonding strength, etc. were investigated. The results from this study can be stated as follows:

(1) Homogeneous ZrO_2/HA composite coatings can be fabricated by plasma spraying, and the ZrO_2 particles distribute uniformly in the HA matrix.
(2) ZrO_2/HA composite coatings contain more unmelted small particles, and the amount of

unmelted particles increases with increase of ZrO_2. Addition of ZrO_2 also causes an increase in porosity of the composite coatings.

(3) ZrO_2 reacts with CaO in HAC to form $CaZrO_3$ during the fabrication process, meanwhile this reaction causes destabilization of HA to decompose into more α-TCP phase.

(4) The cubic phase of TZ3Y and TZ8Y remains stable during plasma spraying.

(5) The bonding strength of HA increases with addition of Y-ZrO_2, and the bonding strength of the TZ3Y reinforced HA increases with increase of TZ3Y content in the range 0 to 10 wt % studied.

(6) The advantageous effect of toughening outweights the adverse effect of increased porosity associated with the incorporation of ZrO_2.

References

1. R. G. T. GEESINK, K. DE GROOT and C. P. A. KLEIN, *Clin. Orthop. Rel. Res.* **225** (1987) 149.
2. K. A. THOMAS and S. D. COOK, *J. Biomed. Mater. Res.* **19** (1985) 875.
3. J. A. JANSEN, J. P. C. M. VAN DE WAERDEN, J. G. C. WOLK and K. DE GROOT, *ibid.* **25** (1991) 973.
4. B. C. WANG, E. CHANG, C. Y. YANG and D. TU, *J. Mater. Sci. Mater. Med.* **4** (1993) 394.
5. M. JARCHO, C. H. BOLEN, M. B. THOMAS, J. BOBICK, J. F. KAY and R. H. DOREMUS, *J. Mater. Sci.* **11** (1976) 2027.
6. C. P. A. T. KLEIN, P. PATKA, H. B. M. VAN DER LUBBE, J. G. C. WOLKE and K. DE GROOT, *J. Biomed. Mater. Res.* **25** (1991) 53.
7. B. C. WANG, T. M. LEE, E. CHANG and C. Y. YANG, *J. Biomed. Mater. Res.* **27** (1993) 1315.
8. Y. MURASE, E. KATO and K. DAIMON, *J. Amer. Ceram. Soc.* **69** (1986) 83.
9. S. R. WITEK, E. D. BUTLER, *J. Mater. Sci. Lett.* **4** (1985) 1412.
10. Q. L. GE, T. C. LEI and Y. ZHOU, *Mater. Sci. and Technol.* **7** (1991) 490.
11. T. KASUGU, M. YOSHIDA, A. J. IKUSHIMA, M. TUCHIYA and H. KUSAKARI, *J. Mater. Sci. Mater. Med.* **4** (1993) 36.
12. K. IOKU, S. SOMIYA and M. YOSHIMURA, *J. Jpn. Ceram. Soc.* **99** (1991) 196.
13. M. TAKAGI, M. MOCHIDA, N. UCHIDA, K. SAITO and K. UEMATSU, *J. Mater. Sci. Mater. Med.* **3** (1992) 199.
14. N. CLAUSSEN, *J. Amer. Ceram. Soc.* **61** (1978) 85.
15. W. J. BRINDLEY and R. A. MILLER, *Adv. Mater. Processes* **8** (1989) 29.
16. S. R. RADIN and P. DUCHEYNE, *J. Mater. Sci. Mater. Med.* **3** (1992) 33.
17. N. TAMARI, M. MOURI and I. KONDO, *J. Jpn. Ceram. Soc.* **95** (1987) 806.
18. J. M. WU and T. S. YEH, *J. Mater. Sci.* **23** (1988) 3771.
19. B. C. WANG, E. CHANG, D. TU and C. H. TSAI, *Surf. Coat. Technol.* **58** (1993) 107.
20. G. C. WEI and P. F. BECHER, *J. Amer. Ceram. Soc.* **67** (1984) 571.
21. R. W. RICE, *Ceram. Engng. Sci. Proc.* **2** (1981) 661.

Received 6 February
and accepted 14 March 1996